Ancillary material

Ziyi Yin[1,*], Rafael Orozco,[1,*], Mathias Louboutin[2], Felix J. Herrmann[1]
[1] Georgia Institute of Technology, [2] Devito Codes Ltd, [*] First two authors contributed equally

1 Summary

This document is structured as follows: First, we provide a more detailed analysis of the case studies on the Compass model. Next, we introduce an additional case study on the CurveFault-A dataset from Open FWI dataset [1].

2 Compass

In the Compass case study, WISE showcases its ability to generate velocity models consistent with the observed shot data. Here, we delve into a detailed analysis of these results in this section to affirm its superior performance. To benchmark WISE against traditional FWI methods, we initiate by conducting FWI on the 1D initial model depicted in Figure 1(b) in the main text. Subsequently, we examine several posterior samples from WISE, focusing on the analysis of CIG focusing.

2.1 Full-waveform inversion from the 1D initial model

We conducted an FWI on the 1D initial model depicted in Figure 1(b) in the main text, using 200 iterations of gradient descent. In each iteration, we selected 4 random OBNs with replacement to determine the update direction. The entire inversion amounts to 12.5 datapasses. To address cycle-skipping, we employed a frequency continuation strategy, progressively inverting data from low to high frequencies [2]. The FWI result, presented in Figure 1(a), reveals mispositioning of several major reflectors and poor recovery of layers beneath the unconformity. This issue becomes more pronounced in the vertical profiles shown in Figure 2. The cycle-skipping problem led to the FWI's failure in accurately estimating the bottom of the velocity "kick-back" layer at approximately $800\,\mathrm{m}$ depth, resulting in mispositioned layers, including the unconformity at about $2200\,\mathrm{m}$ depth. Conversely, the conditional mean estimate from WISE closely matches the ground truth velocity trend, and the 95% confidence interval successfully encompasses the ground truth velocity model at nearly all locations.

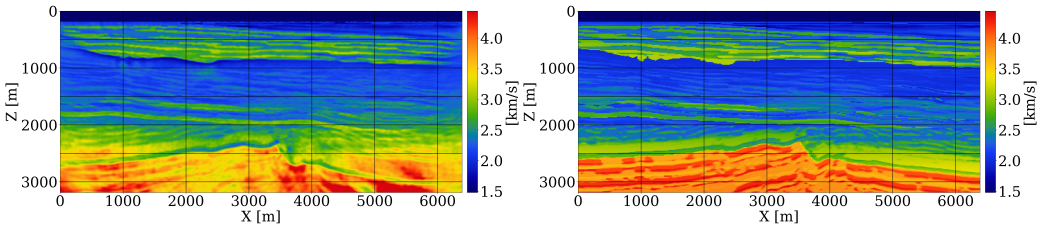

(a) (b)

Figure 1: (a) FWI result using Figure 1(b) in the main text as a starting model; (b) ground truth velocity model.

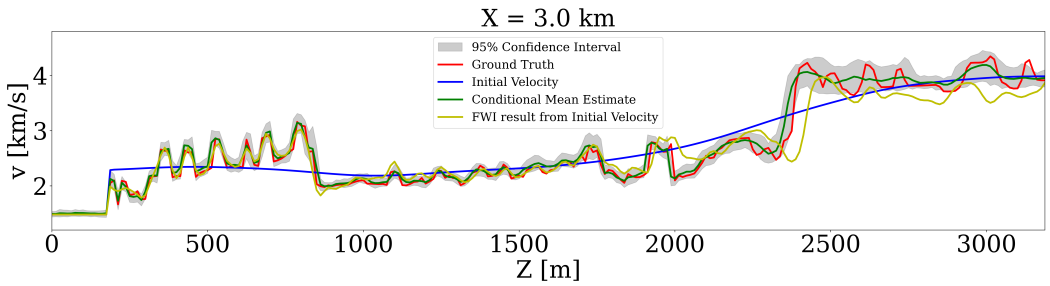

(a)

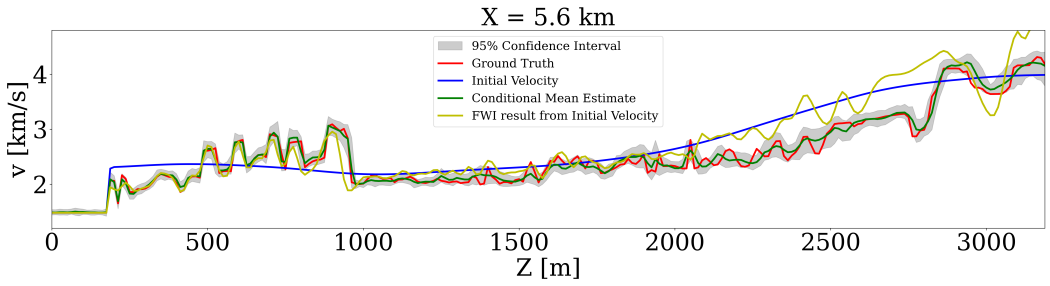

(b)

Figure 2: Vertical profiles.

2.2 Common-image gathers of posterior samples

To evaluate the focusing of CIGs for all posterior samples, we calculated the percentage of energy within near offsets (specifically, between $-60, \mathrm{m}$ and $60, \mathrm{m}$) as $\|\text{energy in near offsets}\|_2 / \|\text{energy in all offsets}\|_2$. The CIGs derived from the initial 1D velocity model (depicted in Figure (1)b of the main text) contained only 73.6% of their energy in near offsets, whereas the conditional mean estimate from WISE (illustrated in Figure (1)d) accounted for 81.6% of the energy. This quantitatively confirms the enhanced focusing of the conditional mean estimate. Moreover, we computed the focused energy percentage in near offsets for CIGs produced by all posterior samples, resulting in an average of 74.3% — an improvement over the initial 1D velocity model. The standard deviation among these measurements was 0.005%. Three CIG examples are presented in Figure 3, which, while not as sharply focused as the conditional mean estimate CIGs (shown in Figure 1(f) in the main text), exhibit visibly better focusing than those generated by the 1D velocity model (shown in Figure 1(e) in the main text). For further analysis, practitioners might choose posterior samples based on this metric or other criteria, such as the curvature of gathers determined by migration velocity analysis. We propose to explore these alternative selection methodologies in future research.

3 Open FWI

We present a case study using the CurveFault-A models in the Open FWI dataset, which is a public deep learning benchmark dataset for FWI. The CurveFault-A dataset comprises velocity models with significant variability across samples, which poses challenges for deep learning methods. This is further compounded by faults and dipping events while observations contain only reflected energy. Testing on this dataset allows us to test WISE's velocity-model generation capabilities.

Dataset generation and network training. We select 2800 velocity models of 640 m by 640 m, each with 64 equally spaced receivers at $10\mathrm{m}$ tow depth and 16 randomly placed sources. The surface is assumed absorbing. Using a $15\mathrm{Hz}$ central frequency Ricker wavelet with energy below $3\mathrm{Hz}$ removed for realism, acoustic data is simulated with Devito [3, 4] and JUDI.jl [5]. Uncorrelated band-limited Gaussian noise is added (S/N $12\mathrm{dB}$) before migrating each dataset with a 1D initial FWI-velocity model calculated by averaging the corresponding true model horizontally. CIGs are computed for 101 horizontal subsurface offsets ranging from $-250\mathrm{m}$ to $+250\mathrm{m}$. Two CNFs are trained: one with velocity-RTM pairs and another with velocity-CIGs pairs.

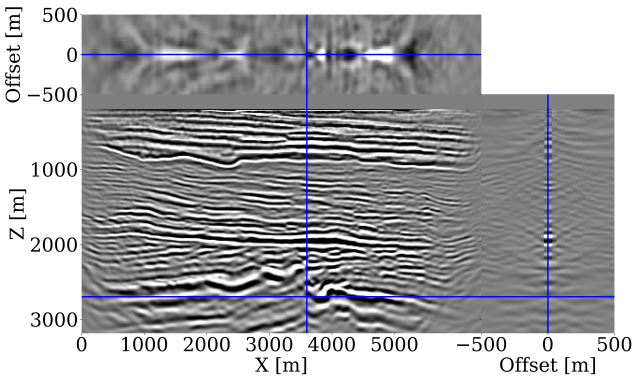

(a)

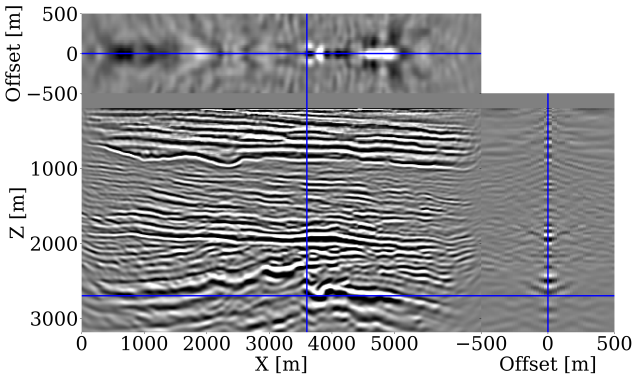

(b)

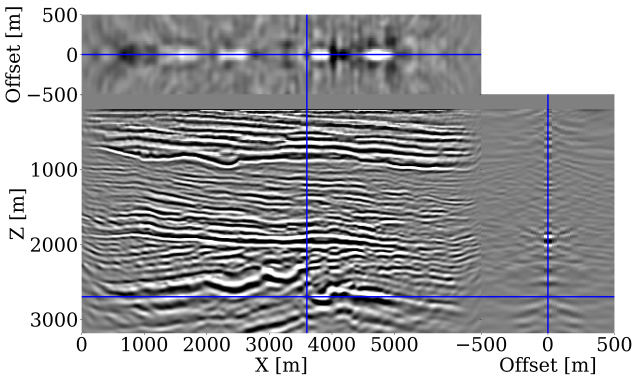

(c)

Figure 3: CIGs for three posterior samples from WISE.

Results. Results on two tested samples by our CNFs are included in Figure 4 and reveal notable variation in the posterior samples for sharp boundaries and smooth transitions in the velocity. While the conditional mean estimate does not fully replicate the true velocity, the standard deviations meaningfully correlate with the errors, indicating that the uncertainty represented by the standard deviation is informative. Across 50 test samples, the mean SSIM score for CIGs-based statistics is 0.87, surpassing the 0.85 mean for RTM-based statistics. We also observe that CIGs better inform the posterior compared to RTM in both test samples.

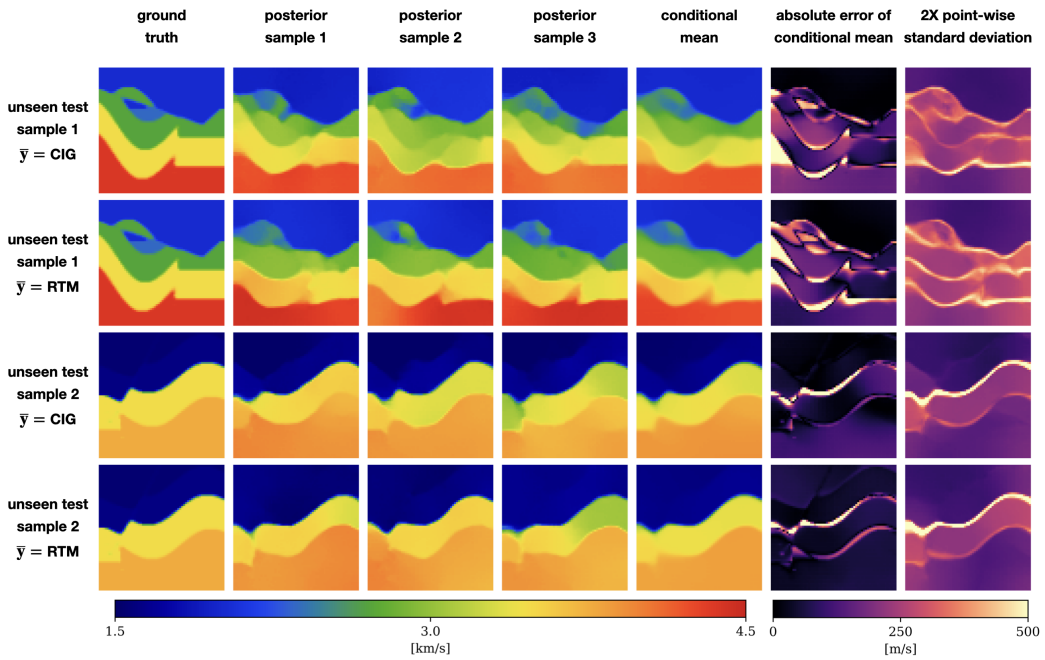

Figure 4: Applying WISE for two unseen test samples in Open FWI CurveFault-A dataset. $\overline{y}$ denotes the type of summary statistics.

References

[1] Chengyuan Deng, Shihang Feng, Hanchen Wang, Xitong Zhang, Peng Jin, Yinan Feng, Qili Zeng, Yinpeng Chen, and Youzuo Lin. Openfwi: Large-scale multi-structural benchmark datasets for full waveform inversion. *Advances in Neural Information Processing Systems*, 35:6007–6020, 2022.

[2] Carey Bunks, Fatimetou M Saleck, S Zaleski, and G Chavent. Multiscale seismic waveform inversion. *Geophysics*, 60(5):1457–1473, 1995.

[3] M. Louboutin, M. Lange, F. Luporini, N. Kukreja, P. A. Witte, F. J. Herrmann, P. Velesko, and G. J. Gorman. Devito (v3.1.0): an embedded domain-specific language for finite differences and geophysical exploration. *Geoscientific Model Development*, 12(3):1165–1187, 2019. doi: 10.5194/gmd-12-1165-2019. URL https://www.geosci-model-dev.net/12/1165/2019/.

[4] Fabio Luporini, Mathias Louboutin, Michael Lange, Navjot Kukreja, Philipp Witte, Jan Hückelheim, Charles Yount, Paul H. J. Kelly, Felix J. Herrmann, and Gerard J. Gorman. Architecture and performance of devito, a system for automated stencil computation. *ACM Trans. Math. Softw.*, 46(1), apr 2020. ISSN 0098-3500. doi: 10.1145/3374916. URL https://doi.org/10.1145/3374916.

[5] Philipp A. Witte, Mathias Louboutin, Navjot Kukreja, Fabio Luporini, Michael Lange, Gerard J. Gorman, and Felix J. Herrmann. A large-scale framework for symbolic implementations of seismic inversion algorithms in julia. *Geophysics*, 84(3):F57–F71, 2019. doi: 10.1190/geo2018-0174.1. URL https://doi.org/10.1190/geo2018-0174.1.